International Journal of
Environmental Research and Public Health

MDPI

Review

Effects of Physicochemical Parameters on Struvite Crystallization Based on Kinetics

Jinzhu Wu [1], Yifan Li [1], Baojian Xu [1], Mei Li [1], Jing Wang [1], Yuanyuan Shao [1], Feiyong Chen [1], Meng Sun [2] and Bing Liu [1,*]

[1] Resources and Environment Innovation Institute, School of Municipal and Environmental Engineering, Shandong Jianzhu University, Jinan 250101, China; wjz408858154@126.com (J.W.); yifan_li2019@163.com (Y.L.); x17865178852@163.com (B.X.); limei@sdjzu.edu.cn (M.L.); jwang@sdjzu.edu.cn (J.W.); shaoyuanyuan@sdjzu.edu.cn (Y.S.); ctokyo@hotmail.com (F.C.)
[2] Faculty of Environmental Engineering, The University of Kitakyushu, 1-1, Hibikino, Wakamatsu, Kitakyushu 802-8577, Japan; m-sun@kitakyu-u.ac.jp
* Correspondence: b-liu@sdjzu.edu.cn

Abstract: The precipitation of struvite ($MgNH_4PO_4 \cdot 6H_2O$) is considered to be a promising method for the recovery of phosphate from wastewater. In this review, the kinetic models, which are commonly used to explain the process of struvite crystallization, are described. The mixed-suspension mixed-product removal (MSMPR) model is based on the population balance equation (the size-dependent growth model and the size-independent growth model). Thereafter, the first-order kinetic fitting model that aligned with concentration changes in the substrate is summarized. Finally, the several physical and chemical factors that affected the efficiency of struvite crystallization are determined. The supersaturation ratio, which is seen as the driving force of struvite crystallization, is the main factor that influences crystallization; however, it cannot be used in practical applications of engineering because it is indirectly associated with the following factors: pH, the molar ratio of Mg:N:P, and the interference of foreign impurities. In this study, we present conclusions that should be used to guide further research studies, and encourage the engineering practice of wastewater treatment with struvite precipitation.

Keywords: phosphate recovery; struvite; chemical precipitation; crystallization kinetics

Citation: Wu, J.; Li, Y.; Xu, B.; Li, M.; Wang, J.; Shao, Y.; Chen, F.; Sun, M.; Liu, B. Effects of Physicochemical Parameters on Struvite Crystallization Based on Kinetics. *Int. J. Environ. Res. Public Health* **2022**, *19*, 7204. https://doi.org/10.3390/ijerph19127204

Academic Editor: Shihong Zeng

Received: 6 May 2022
Accepted: 9 June 2022
Published: 12 June 2022

1. Introduction

Phosphorus is a limiting nutrient in organisms of an ecosystem. Whenever there is an excessive discharge of phosphorus in the ecosystem, it leads to eutrophication of water and causes environmental damage [1]. Although the reserves of phosphorus are limited and nonrenewable, the consumption of phosphorus has increased steadily in recent decades [2,3]. Therefore, it is essential to recycle the resources of phosphorus and to gain social and economic benefits [4]. The recovery of phosphate is achieved by crystallizing struvite ($MgNH_4PO_4 \cdot 6H_2O$), which is an important phosphate mineral found in wastewater [5]. The recovery of phosphate is possible from this mineral because the phosphate removal rate is excellent in the crystallization process. Furthermore, the isolated phosphate can be fixed as a fertilizer, thereby enhancing its economic value [6,7]. Traditional phosphorus fertilizers are mostly water soluble. Phosphorus in farmland enters rivers with precipitation and drainage, resulting in eutrophication of a water body and lack of phosphorus in the later stage of crop growth. Different from traditional fertilizers, struvite has low solubility in water and is not prone to leaching loss [8]. It is a slow-release phosphate fertilizer. Struvite was first found in a sludge digestion system [9,10]. It is a crystal formed by chelating equimolar concentrations of magnesium, ammonium, and phosphate with six water molecules [11]. The crystallization process can be completed in

less than one minute. The crystallization of struvite is favored as its solubility is low in water. The solubility product constant of struvite (Ksp) is 13.26 in water [12].

The crystallization of struvite is a complex process, which is affected by the following physicochemical parameters: pH, the molar ratio of Mg:N:P, temperature, and foreign impurities [13,14]. Therefore, the various physicochemical parameters that influence the process of struvite crystallization need to be understood. In many current studies, phosphorus removal rate has been used to characterize the effects of various physicochemical parameters on struvite crystallization. However, the key to phosphorus recovery not only needs high phosphorus removal rate, but also needs to form high-quality struvite. Therefore, the model of struvite crystallization needs to be established to investigate the effect of physicochemical parameters on the nucleation and growth of struvite from the perspective of kinetics. With this knowledge, highly pure struvite was synthesized, which can be further used for highly efficient phosphate recovery [15]. In addition, struvite crystallization is favored by establishing the proper equilibrium and growth rate of crystals. Thus, the uncertainty can be reduced in the process, design, and operation of crystallization units [16].

Currently, the dynamic kinetics of struvite crystallization are described by the following models: the population density model [17], the surface growth model [18], and the first-order dynamic model of substrate concentration [19]. Furthermore, the population density model describes how the total rate of change in the crystal number occurs due to variations in following parameters: diameter, surface area, volume, shape, etc.

The objective of this study is to summarize the common kinetic models used in struvite crystallization. Thereafter, the effects of various physical and chemical parameters on the crystallization efficiency of struvite are discussed. Subsequently, the results were used to understand the perspective of crystallization kinetics, which can be further used as a reference work in the development of an efficient technology for phosphate recovery.

2. Model of Struvite Crystallization

In wastewater, supersaturated magnesium ions (Mg^{2+}), ammonium (NH_4^+), and orthophosphate (PO_4^{3-}, HPO_4^{2-} and $H_2PO_4^-$) combine to form struvite ($MgNH_4PO_4{\cdot}6H_2O$). Struvite is formed through the following equation [20]:

$$Mg^{2+} + NH_4^+ + PO_4^{3-} + 6H_2O \rightarrow MgNH_4PO_4{\cdot}6H_2O \quad (1)$$

The driving force (F) of struvite crystallization is defined as follows [21]:

$$F = -\frac{R_g T}{\alpha} \ln \Omega \quad (2)$$

where R_g is the gas constant (8.31 $J{\cdot}K^{-1}{\cdot}mol^{-1}$); α is 3; T is the absolute temperature; and Ω is the supersaturation ratio of the solution, which is defined as the ratio of the ion activity product (IAP) in the solution to the solubility product (K_{sp}) of the struvite crystal.

$$\Omega = \frac{(Mg^{2+})(NH_4^+)(PO_4^{3-})}{K_{sp}} \quad (3)$$

where $\left(Mg^{2+}\right)$ $\left(NH_4^+\right)$ $\left(PO_4^{3-}\right)$ denotes the activity of Mg^{2+}, NH_4^+, and PO_4^{3-} ions in the solution, and it is calculated by using the Davies model; and K_{sp} is the solubility product of struvite crystal.

The crystallization process of struvite is classified into two primary stages: the nucleation and the growth of crystals. In the nucleation phase, the ions combine with each other to form a crystalline embryo. The growth of crystals ends when an equilibrium is reached in the reaction mixture [14]. In general, nucleation is classified into two types: homogenous nucleation is a spontaneous process; heterogeneous nucleation is brought

about by including suspended solid impurities in the solution [22]. According to classical nucleation theory, the homogenous nucleation rate J can be calculated as follows [23]:

$$J = \delta \exp\left(-\frac{\beta\gamma^3 v^2}{(kT)^3(\ln\Omega)^2}\right) \quad (4)$$

where β is a shape factor; v is the molecular volume; γ is the surface energy of the crystal; k is the Boltzmann's constant (1.381×10^{-23} J/K); and δ is the pre-exponential factor [24].

$$\delta = \left(\frac{D}{d^5 N}\right)\left(\frac{4\Delta G}{3\pi kT}\right)^{1/2} \quad (5)$$

where D is the diffusion coefficient; d is the interplanar distance of the crystalline lattice; N is the number of molecules that form a critical sized nucleus; and ΔG is the change in Gibb's free energy, which occurs due to the formation of a critical nucleus.

The induction time of a crystal is defined as the time expended from the supersaturation of the solution to the solid formation; it can be determined from the changes caused by crystallization in solution properties such as pH and conductivity [18]. By assuming that the induction time is much lesser than the nucleation time, the induction time (τ) was determined as follows:

$$\tau = \frac{A}{(\log\Omega)^2} - B \quad (6)$$

where $A = \beta\gamma^3 v^2/(2.303\,kT)^3$ and $B = \log\xi$.

The growth rate of struvite crystals is calculated by using the following equation:

$$R = k_r(\Omega^{\frac{1}{3}} - 1)^n \quad (7)$$

where k_r is the reaction coefficient; and n is the apparent reaction order.

In previous studies, researchers have determined the kinetics of struvite crystallization by using the mixed-suspension mixed-product removal (MSMPR) model. This model is based on the population balance equation. It is a method used to estimate the kinetic parameters of the crystallization of struvite, which depend on the crystal size distribution (CSD) of the product [17,25,26]. The crystal growth rate and nucleation rate affect CSD in solution, which is the key to control the quality of struvite [27]. The MSMPR model includes the size-dependent growth (SDG) model and the simplified size-independent growth model (SID).

In the MSMPR model, the population density of the mean size of struvite crystal $n_i(L_i)$ is based on CSD data. The model is described by the following equation [17]:

$$n_i(L_i) = \frac{m_i(L_i)}{k_v \rho L_i^3 \Delta L_i V_w} = \frac{V_i(L_i)}{k_v L_i^3 \Delta L_i V_w} \quad (8)$$

where L_i denotes the mean size of the ith crystal; m_i is the mass of the crystal; V_i is the volume of the crystal; k_v is the shape factor; ρ is the density of the crystal; ΔL_i denotes the crystal size range; and V_w is the total volume of the system.

Using the assumption of the SID model, we calculated the linear growth rate G of the crystal by the following equation:

$$\ln n(L) = -\frac{L}{tG} + \ln n_0 \quad (9)$$

where t is the mean retention time of the crystal; $\ln n(L)$ has a linear relationship with L, and its slope is 1 /tG. After determining the value of t, G is obtained by fitting the slope of

the straight line. The intercept of the fitting line is denoted as $\ln n_0$. The nucleation rate (B) can be written according to the following equation [25]:

$$B = n_0 G \tag{10}$$

Since the crystals are of different sizes, their growth rates are also different [28]. Therefore, the SDG model is introduced, and its parameters are defined in Table 1:

Table 1. The SDG models.

Linear Growth Rate G	Mean Size Population Density n (L)	References
$G = G_0 \left(1+\frac{L}{tG_0}\right)^b$ $b < 1$	$n(L) = n_0\left(1+\frac{L}{tG_0}\right)^{-b} \exp\left[\frac{1}{1-b} - \frac{\left(1+\frac{L}{tG_0}\right)^{-b}}{1-b}\right]$	[29]
$G = G_m\left(1-e^{-a(L+c)}\right)$ $a > 0, c \neq 0$	$n(L) = n_0 e^{aL}\left(\frac{e^{a(L+c)}-1}{e^{ac}-1}\right)^{(-1-atG_m)/atG_m}$	[30]
$G = G_m\frac{e^{aL}-b}{e^{aL}-c}$	$n(L) = n_0\left(\frac{e^{aL}-c}{1-c}\right)\left(\frac{e^{aL}-b}{1-b}\right)^{\frac{c-a-abtG_m}{abtG_m}} e^{-\frac{cL}{btG_m}}$	[31]
$G = G_m - (G_m - G_0)e^{aL}$	$n(L) = n_0 e^{\frac{L}{tG_m}}\left(\frac{G_0}{G_m-(G_m-G_0)e^{aL}}\right)^{\frac{1}{atG_m}+1}$	[32]

where G_0 represents the linear growth rate of nuclei, which further grow into zero-size crystals; G_m represents the limiting linear growth rate of most giant crystals; a, b, and c represent the empirical constants.

The SIG model is a simplification of the SDG model, which is only used to process the growth data of smaller crystals, but it should be noted that the simulation of G(SIG) and G_m (SDG) by the two models is similar [33].

The first-order kinetic model is used to assess the growth rate of struvite crystallization, which can be further described as follows [19,34]:

$$\ln(C - C_{eq}) = -kt + \ln(C - C_0) \tag{11}$$

where C is the concentration of the substrate at time t; C_{eq} is the equilibrium concentration of the substrate; C_0 is initial concentration of substrate; and k is the rate constant of first-order reaction. The parameter values in some studies are summarized in Table 2.

Table 2. An overview of previous kinetics studies of struvite crystallization.

Research Object	pH (−)	Temperature °C	Molar Ratio (Mg:p)	k (min^{-1})	R^2 (−)	References
Phosphate concentration	7.5	22–25	1.5	0.039	>0.92	[35]
Phosphate concentration	8.51	20	1.6	0.045	0.97	[36]
Phosphate concentration	8.4	22–24	1.2	0.061	0.96	[37]
Magnesium concentration	9.0	30	1.0	0.109	0.99	[19]
Magnesium concentration	9.0	20	0.5	0.156	>0.92	[38]

It should be noted that most kinetic studies regard the crystallization of struvite as a first-order irreversible reaction. In fact, the crystallization behavior of struvite is reversible [39].

In addition, the reaction order method [40] and the chemical potential gradient model [41] were used to simulate the rate of struvite crystallization, providing new insights into the crystallization behavior of struvite.

3. The Parameters That Influence Struvite Crystallization

Supersaturation is a crucial factor that affects the rate of struvite crystallization. However, it should be emphasized that supersaturation is indirectly affected by the following factors: pH, concentration of the solute, temperature, and the presence of foreign impurities in the solution. Due to these factors, supersaturated crystals of struvite cannot be used in

practical applications of engineering. In this section, how the aforementioned factors affect the formation of struvite crystals is summarized.

3.1. pH

The dissolution and crystallization of struvite occur simultaneously in an aqueous solution [42]. Initially, the solubility of struvite decreases, but it increases when the pH value increases subsequently [43]. The solubility of struvite is minimum when the pH value is maintained between 8.5 and 9.0 [44]. In acidic conditions, struvite decomposes to form an amorphous crystal. At this stage, the concentration of $H_2PO_4^-$ ions decreases [45]. Furthermore, when the pH is increased above the value of 9, the solubility of struvite starts increasing. This happens when ionized ammonium ion (NH_4^+) is converted into an unionized state of ammonia (NH_3), causing a decrease in supersaturation [46].

In solutions with different pH, the ion concentration profiles of orthophosphate and ammonia are different. This implies that the supersaturation ratio of the solution is affected by pH, causing changes in the growth rates of struvite crystals. When the pH value of the solution is 8.0, 8.5, and 9.0, the kinetics of struvite crystals growth follows a first-order equation. Its first-order rate constants are 3.7, 5.1, and 6.9 h^{-1} at pH values of 8.0, 8.5, and 9.0, respectively [47]. Moreover, the first-order rate constant of struvite crystals growth increases when the pH value is increased from 8.4 to 9.0 [37].

The zeta potential is affected by the interaction between particles in an aqueous solution. A change in pH of the solution can change the value of the zeta potential, thereby affecting the growth kinetics of the struvite crystal. When the pH value is increased steadily, the zeta potential becomes more negative. Consequently, the growth rate of crystals is accelerated in the solution [23,48]. However, if the initial value of pH is high, the positive zeta potential is high, and the nucleation time is increased substantially [24].

The pH value is varied to modify the shape and the linear growth rate of struvite crystals. By increasing the pH value, the size and the thickness of struvite crystal are decreased. Matynia, et al. [49] reported that when the pH value of the solution increased from 8 to 10, the average crystal size of struvite decreased by 5.5 times. Similarly, in the study of Anna, et al. [50], the average crystal size of struvite decreased by 3 times when the pH value of the solution increased from 9 to 11. Mazienczuk, et al. [25] reported that when the range of pH values was controlled within 9–11, the relationship between crystal size, linear growth rate, and pH value was as follows:

$$L_m = 2.86 \times 10^5 pH^{-5.44} t^{0.328} \quad R^2 = 0.808 \tag{12}$$

$$G = 5.39 \times 10^{-4} pH^{-2.99} t^{0.683} \quad R^2 = 0.905 \tag{13}$$

In addition, Mg^{2+} ions form crystals of Mg $(OH)_2$ salt at higher pH values. This supplementary crystallization process interferes with the formation of struvite crystals. Primarily, if the pH value is greater than 10.5, a $Mg_3(PO_4)_2$ compound is formed, and it is insoluble in a strongly alkaline environment [51]. The crystallization of $Mg_3(PO_4)_2$ and $Mg(OH)_2$ is described by the following equations [52]:

$$3Mg^{2+} + 2PO_4^{3-} \rightarrow Mg_3(PO_4)_2 \tag{14}$$

$$Mg^{2+} + 2H_2O \leftrightarrow Mg(OH)_2 \downarrow + 2H^+ \tag{15}$$

In summary, the effect of pH on struvite crystallization is summarized as follows: Firstly, the pH value affects the formation of new ion species in the solution, which encourages the formation of other crystals. Secondly, it affects the solubility and zeta potential of struvite crystals. When the pH value of the solution is less than 7, there is formation of mainly orthophosphate $H_2PO_4^-$. At this acidic pH value, the crystallization and the growth of struvite are significantly inhibited. However, at a high pH value ($\geq$11), other precipitates are formed and ammonia becomes volatized. These events lead to the dissolution of struvite, and the nucleation and crystallization of struvite are inhibited. In addition, as the pH

value of solution increases, the nucleation rate increases in struvite crystals and the growth rate of struvite crystals decreases, which produces a large number of small-sized struvite.

3.2. Molar Ratio of Mg:N:P

As shown in Equation (1), the theoretical molar ratio of Mg:P:N is 1:1:1. However, to ensure that phosphorus is removed with high efficiency, an excessive amount of ammonium or magnesium or both elements is often added. In a study conducted by Gong, et al. [53], the molar ratio of Mg:P was increased from 0.8 to 1.2. Consequently, the rate of phosphorus removal increased from 80.8 to 95.5%. This is because other insoluble compounds of magnesium and phosphorus were formed along with struvite crystals [54]. Similarly, Hutnik et al. [55] reported that the addition of excess magnesium ion is not only conducive to the formation of larger struvite crystals, but also can remove a variety of impurities in wastewater. Furthermore, at a given value of pH, an excessive concentration of phosphorus was maintained. In these conditions, the degree of supersaturation depended only on the concentration of magnesium and ammonium ions [56]. The yield of struvite increased when the concentration of Mg^{2+} and $NH_4{}^+$ was increased. This indicates that the saturation of struvite is directly proportional to the logarithm of the ionic concentrations in the crystal [57].

The molar ratio of Mg:N:P elements affect the supersaturation, which further impacts the crystalline morphology of struvite. When the relative supersaturation ratio σ ($\Omega^{1/3} - 1$) is within the range of 1.0–1.5, the struvite crystal develops into the shape of a coffin. When the relative supersaturation ratio is within the range of 1.5–3.0, the struvite crystal possesses a twin/polycrystalline state and develops into an X-shaped and needle-like shaped crystal [58]. In addition, the kinetic parameters of struvite crystallization are affected by supersaturation. Galbraith et al. [59] reported that struvite crystals more likely aggregate with supersaturation increases. Similarly, Koralewska et al. [60] reported that when Mg^{2+} increased from 0.1 to 1 mass-%; Gm and G_0 of struvite crystal increased from 8.38×10^{-9}, 1.48×10^{-10} to 1.18×10^{-8}, 6.62×10^{-10} m/s; and B from 6.22×10^{12} to $4.67 \times 10^{14}/m^3 \cdot s$. Higher supersaturation is beneficial to the nucleation and growth of struvite, and leads to a faster precipitation process and greater particle density.

3.3. The Effects of Foreign Impurities on Struvite Crystallization

It is established that Ca^{2+} or $CO_3{}^{2-}$ ions extend the induction time of crystallization and inhibit the growth rate of crystals. When calcium ions are absorbed on the surface of a crystal, the binding site of ammonia is occupied. Consequently, the crystallization of struvite is inhibited [61]. Furthermore, calcium ions can consume phosphate and then influence an oversaturated form of struvite. Calcium ions interact with phosphate or carbonate ions to form calcium phosphate (usually hydroxyapatite) or calcium carbonate (usually calcite), respectively. Please refer to Equations (16) and (17) [62]:

$$5Ca^{2+} + 3PO_4^{3-} + H_2O \rightarrow Ca_5(PO_4)_3OH + H^+ \quad (16)$$

$$Mg^{2+} + 2H_2O \leftrightarrow Mg(OH)_2 \downarrow + 2H^+ \quad (17)$$

Yaakoubi et al. [63] reported that the reaction processes of struvite crystallization were dramatically improved when Ca^{2+} or Mg^{2+} ions were added into an aqueous solution containing phosphate and ammonia species. As shown in Figure 1, precipitates of $CaHPO_4 \cdot 2H_2O$ and $MgHPO_4 \cdot 3H_2O$ were obtained initially due to high solubility and weak thermodynamics. Subsequently, a more stable form of the species was generated as $CaHPO_4$ and $Mg_3(PO_4)_2 \cdot 8H_2O$. In the same manner, $Ca_3(PO_4)_2$ and Mg (NH_4) $PO_4 \cdot 6H_2O$ were eventually achieved.

In a study conducted by Hutnik et al. [26], the SDG model was used to determine how calcium ions affect the crystallization of struvite. When the concentration of calcium ions was increased from 100 mg/L to 2000 mg/L, the nuclear growth rate decreased significantly from 2.30×10^{-11} to 2.09×10^{-12} m/s. Moreover, the linear growth rate of

crystals also decreased significantly from 1.71×10^{-8} to 9.10×10^{-9} m/s. Nevertheless, the nucleation rate of struvite increased 160 times. In contrast, the purity of struvite decreased by 8.1 mass%. Moreover, the process of struvite crystallization slowed down when the molar ratio of Ca^{2+}/Mg^{2+} ions became greater than 0.2. The formation of struvite crystals was significantly inhibited, and the purity decreased when the molar ratio was increased from 0.5 to 1.0. Moreover, the formation and the purity of struvite crystals declined when the molar ratio of Ca^{2+}/PO_4^{3-} was increased from 0.5 to 1.0 [20].

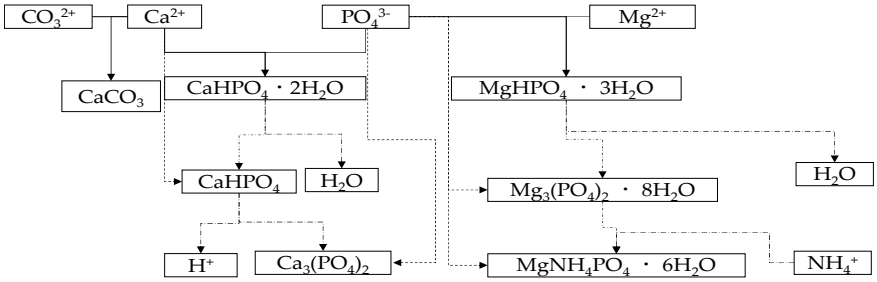

Figure 1. Reaction map of calcium and magnesium with soluble phosphate (−: primary solid crystallization; − · −: transform to a secondary solid; − − −: precipitate of the secondary solid).

The nucleation and growth of struvite crystals improve with the presence of copper ions in the solution. This is because copper ions increase the linear growth rate of struvite crystals. In contrast, they also cause a decline in the nucleation rate, thereby facilitating the formation of large-sized crystals [64]. A similar phenomenon was observed when the solution was treated with aluminum ions. When the concentration of aluminum ions was increased from 10 to 100 mg/L, the nucleation rate of struvite decreased by 5%. In contrast, the linear growth rate of struvite crystals increased by 8%, and the average size of crystals increased by 22% [17]. In addition, Hutnik et al. [65] reported that the existence of K^+ increases the growth rate of struvite crystal, and the average size of struvite was about 46 um.

Magnesium chloride is often used as a source of magnesium and an additive. Ariyanto, et al. [14] determined how chloride ions affect the crystallization efficiency of struvite. The results indicate that excessive chloride ions increase the activation energy of struvite nucleation. Moreover, they also increase the induction time of struvite. Ping, et al. [66] reported that the efficiency of phosphorus removal increased when the total suspended solids were present at higher concentrations in actual wastewater, and the diameter and purity of struvite crystals decreased significantly.

The presence of humic acid in wastewater clearly restricted the removal of phosphate, and the removal efficiency dropped from 97.47% to 80.80% [67]. This is because humic acid contains several carboxylic groups (-COOH). Therefore, humic acid shows a higher affinity towards Mg^{2+} and NH_4^+ ions, facilitating the formation of the following complexes: $[C_3H_5O(COO)_3]_2Mg_3$ and $C_3H_5O(COO)_3(NH_4)_3$ [68]. In addition, Qi Zhang, et al. [69] indicated that the crystallization of struvite was inhibited by the presence of impurities, which were formed when the dissolved humic acid combined with the seed crystal. Moreover, humic acid also endorsed a simple coverage of the available sites on the crystal nucleus, which slowed down the crystallization rate of struvite. The morphology of the collected struvite crystals changed from a prismatic to pyramidal shape because co-crystallization occurred due to the presence of humic acid on the surface of crystals [70]. This point of view is also supported by Wei, et al. [21], who reported that the change in the morphology of crystals was most likely triggered by the following functional groups: amides, humic acid-Mg^{2+} complex, and phosphate ester. These chemical moieties were formed due to the interaction between humic acid and struvite crystals. As shown in Figure 2, foreign impurities have a significant influence on the formation of struvite crystals.

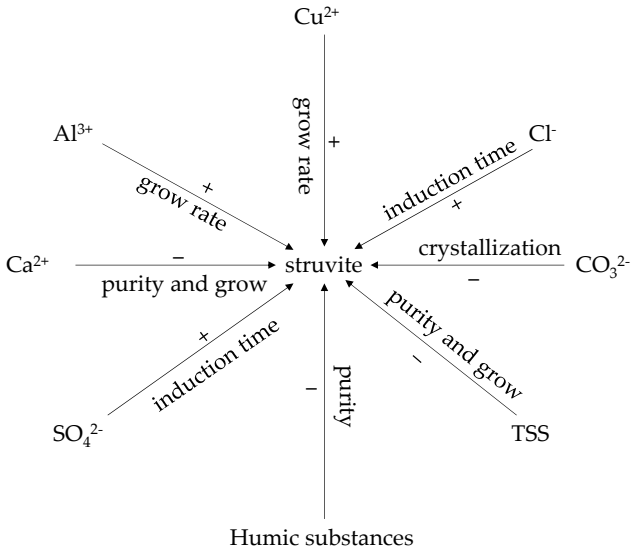

Figure 2. The influence of foreign impurities on struvite: +: positive effect, −: negative effect.

In summary, the effect of foreign impurities on struvite crystallization is complex, and its mechanism needs to be further studied. However, it can be noted that metal cations lead to the decrease in the nucleation rate and the increase in the growth rate of struvite.

4. Conclusions

In this study, the kinetic model of struvite crystallization was explained. The MSMPR model, which is based on a statistical method, can be used to accurately predict the nucleation and crystallization of struvite; however, it cannot describe the mechanism of crystallization. The kinetic model of struvite crystallization needs to be further elucidated.

The lower the nucleation rate, the higher the linear growth rate of crystals; these conditions are considered to be ideal for struvite crystallization. Moreover, the supersaturation rate also needs to be controlled in this process. The supersaturation ratio of the solution is affected by the following parameters: pH, the molar ratio of Mg:N:P elements, and the interference of external ions. All these factors also affect the nucleation and growth rate of struvite crystals.

Author Contributions: Conceptualization, B.L.; methodology, M.L.; investigation, J.W. (Jinzhu Wu), Y.L. and B.X.; Writing—original draft, J.W. (Jinzhu Wu) and J.W. (Jing Wang); Writing—review and editing, M.S. and Y.S. supervision, F.C. All authors have read and agreed to the published version of the manuscript.

Funding: This study was supported by the National science foundation of Shandong Province (No. ZR2020ME236), National key research and development program (2022YFE0105800), Research and development project of the Ministry of housing and urban rural development (K20210424), Science Foundation of Shandong Jianzhu University Grant (No. XNBS1824).

Institutional Review Board Statement: Not applicable.

Informed Consent Statement: Not applicable.

Data Availability Statement: Not applicable.

Conflicts of Interest: The authors declare no conflict of interest.

References

1. Chen, P.; Wu, J.; He, Y.; Zhang, Y.; Yu, R.; Lu, X. Enhanced Nutrient Removal in A2N Effluent by Reclaimed Biochar Adsorption. *Int. J. Environ. Res. Public Health* **2022**, *19*, 4016. [CrossRef] [PubMed]
2. Kim, D.W.; Yu, S.I.; Im, K.; Shin, J.; Shin, S.G. Responses of Coagulant Type, Dosage and Process Conditions to Phosphate Removal Efficiency from Anaerobic Sludge. *Int. J. Environ. Res. Public Health* **2022**, *19*, 1693. [CrossRef] [PubMed]
3. Nur, T.; Loganathan, P.; Kandasamy, J.; Vigneswaran, S. Phosphate Adsorption from Membrane Bioreactor Effluent Using Dowex 21K XLT and Recovery as Struvite and Hydroxyapatite. *Int. J. Environ. Res. Public Health* **2016**, *13*, 277. [CrossRef] [PubMed]
4. Gaterell, M.R.; Gay, R.; Wilson, R.; Gochin, R.J.; Lester, J.N. An Economic and Environmental Evaluation of the Opportunities for Substituting Phosphorus Recovered from Wastewater Treatment Works in Existing UK Fertiliser Markets. *Environ. Technol. Lett.* **2017**, *21*, 1067–1084. [CrossRef]
5. Li, B.; Huang, H.M.; Boiarkina, I.; Yu, W.; Young, B.R. Phosphorus recovery through struvite crystallisation: Recent developments in the understanding of operational factors. *J. Environ. Manag.* **2019**, *248*, 109254. [CrossRef]
6. Farrow, C.; Crolla, A.; Kinsley, C.; Mcbean, E. Ammonia removal from poultry manure leachate via struvite precipitation: A strategy for more efficient anaerobic digestion. *Int. J. Environ. Technol. Manag.* **2017**, *20*, 87–100. [CrossRef]
7. Daneshgar, S.; Callegari, A.; Capodaglio, A.G.; Vaccari, D. The Potential Phosphorus Crisis: Resource Conservation and Possible Escape Technologies: A Review. *Resources* **2018**, *7*, 37. [CrossRef]
8. Benjannet, R.; Nyiraneza, J.; Khiari, L.; Cambouris, A.; Ziadi, N. Potato response to struvite in comparison with conventional phosphorus fertilizer in Eastern Canada. *Agron. J.* **2020**, *112*, 1360–1376. [CrossRef]
9. Rawn, A.M.; Banta, A.P.; Pomeroy, R. Multiple-Stage Sewage Sludge Digestion. *Am. Soc. Civ. Eng.* **1939**, *104*, 93–119. [CrossRef]
10. Rivadeneyra, A.; Gonzalez-Martinez, A.; Gonzalez-Lopez, J.; Martin-Ramos, D.; Martinez-Toledo, M.V.; Rivadeneyra, M.A. Precipitation of Phosphate Minerals by Microorganisms Isolated from a Fixed-Biofilm Reactor Used for the Treatment of Domestic Wastewater. *Int. J. Environ. Res. Public Health* **2014**, *11*, 3689–3704. [CrossRef]
11. Kumari, S.; Jose, S.; Tyagi, M.; Jagadevan, S. A holistic and sustainable approach for recovery of phosphorus via struvite crystallization from synthetic distillery wastewater. *J. Clean. Prod.* **2020**, *254*, 120037. [CrossRef]
12. Iaconi, C.D.; Pagano, M.; Ramadori, R.; Lopez, A. Nitrogen recovery from a stabilized municipal landfill leachate. *Bioresour. Technol.* **2010**, *101*, 1732–1736. [CrossRef] [PubMed]
13. Bayuseno, A.P.; Schmahl, W.W. Crystallization of struvite in a hydrothermal solution with and without calcium and carbonate ions. *Chemosphere* **2020**, *250*. [CrossRef] [PubMed]
14. Ariyanto, E.; Ang, H.M.; Sen, T.K. Impact of various physico-chemical parameters on spontaneous nucleation of struvite ($MgNH_4PO_4{\cdot}6H_2O$) formation in a wastewater treatment plant: Kinetic and nucleation mechanism. *Desalination Water Treat.* **2014**, *52*, 6620–6631. [CrossRef]
15. Almatouq, A.; Babatunde, A.O. Concurrent Phosphorus Recovery and Energy Generation in Mediator-Less Dual Chamber Microbial Fuel Cells: Mechanisms and Influencing Factors. *Int. J. Environ. Res. Public Health* **2016**, *13*, 375. [CrossRef]
16. Burns, M.; Schneider, P.A.; Sheehan, M. Nucleation and crystal growth kinetic parameter optimization of a Continuous Poiseuille flow struvite crystallizer using a discretized population balance and dynamic fluid model. *Chem. Eng. J.* **2020**, *405*, 126607. [CrossRef]
17. Hutnik, N.; Stanclik, A.; Piotrowski, K.; Mat Yn Ia, A. Kinetic conditions of struvite continuous reaction crystallisation from wastewater in presence of aluminium(III) and iron(III) ions. *Int. J. Environ. Pollut.* **2018**, *64*, 358. [CrossRef]
18. Bhuiyan, M.; Mavinic, D.S.; Beckie, R.D. Nucleation and growth kinetics of struvite in a fluidized bed reactor. *J. Cryst. Growth* **2008**, *310*, 1187–1194. [CrossRef]
19. Bayuseno, A.P.; Perwitasari, D.S.; Muryanto, S.; Tauviqirrahman, M.; Jamari, J. Kinetics and morphological characteristics of struvite (MgNH4PO4.6H2O) under the influence of maleic acid. *Heliyon* **2020**, *6*, e03533. [CrossRef]
20. Tao, W.; Fattah, K.P.; Huchzermeier, M.P. Struvite recovery from anaerobically digested dairy manure: A review of application potential and hindrances. *J. Env. Manag.* **2016**, *169*, 46–57. [CrossRef]
21. Wei, L.; Hong, T.; Cui, K.; Chen, T.; Zhou, Y.; Zhao, Y.; Yin, Y.; Wang, J.; Zhang, Q. Probing the effect of humic acid on the nucleation and growth kinetics of struvite by constant composition technique. *Chem. Eng. J.* **2019**, *378*, 122130. [CrossRef]
22. Corona, F.; Hidalgo, D.; Martín-Marroquín, J.M.; Antolín, G. Study of the influence of the reaction parameters on nutrients recovering from digestate by struvite crystallisation. *Environ. Sci. Pollut. Res.* **2020**. [CrossRef] [PubMed]
23. Bouropoulos, N.C.; Koutsoukos, P.G. Spontaneous precipitation of struvite from aqueous solutions. *J. Cryst. Growth* **2000**, *213*, 381–388. [CrossRef]
24. Fromberg, M.; Pawlik, M.; Mavinic, D.S. Induction time and zeta potential study of nucleating and growing struvite crystals for phosphorus recovery improvements within fluidized bed reactors. *Powder Technol.* **2019**, *360*, 715–730. [CrossRef]
25. Mazienczuk, A.; Matynia, A.; Piotrowski, K.; Wierzbowska, B. Continuous Reaction Crystallization of Struvite in a DTM Type Crystallizer With Jet Pump of Ascending Suspension Flow in a Mixing Chamber–Kinetic Approach of the Process. *J. Cryst. Process Technol.* **2012**, *02*, 96–104. [CrossRef]
26. Hutnik, N.; Stanclik, A.; Piotrowski, K.; Matynia, A. Size-dependent growth kinetics of struvite crystals in wastewater with calcium ions. *Open Chem.* **2020**, *18*, 196–206. [CrossRef]
27. Mehta, C.M.; Batstone, D.J. Nucleation and growth kinetics of struvite crystallization. *Water Res.* **2013**, *47*, 2890–2900. [CrossRef]

28. Srisanga, S.; Flood, A.E.; Galbraith, S.C.; Rugmai, S.; Soontaranon, S.; Ulrich, J. Crystal Growth Rate Dispersion versus Size-Dependent Crystal Growth: Appropriate Modeling for Crystallization Processes. *Cryst. Growth Des.* **2015**, *15*, 2330–2336. [CrossRef]
29. Garside, J.; Jani, S.J. Prediction and measurement of crystal size distributions for size-dependent growth. *Chem. Eng. Sci.* **1978**, *33*, 1623–1630. [CrossRef]
30. Jones, J. On the estimation of size-dependent crystal growth rate functions in MSMPR crystallizers. *Chem. Eng. J. Biochem. Eng. J.* **1993**, *53*, 125–135. [CrossRef]
31. Mydlarz, J. An Exponential-Hyperbolic Crystal Growth Rate Model. *Cryst. Res. Technol.* **1995**, *30*, 747–761. [CrossRef]
32. Rojkowski, Z. New empirical kinetic equation of size dependent crystal growth and its use. *Krist. Und Tech.* **1977**, *12*, 1121–1128. [CrossRef]
33. Stanclik, A.; Hutnik, N.; Piotrowski, K.; Matynia, A. Struvite nucleation and crystal growth kinetics from cattle liquid manure. *Chem. Pap.* **2019**, *73*, 555–563. [CrossRef]
34. Perwitasari, D.S.; Muryanto, S.; Jamari, J.; Bayuseno, A.P. Kinetics and morphology analysis of struvite precipitated from aqueous solution under the influence of heavy metals: Cu^{2+}, Pb^{2+}, Zn^{2+}. *J. Environ. Chem. Eng.* **2018**, *6*, 37–43. [CrossRef]
35. Quintana, M.; Sánchez, E.; Colmenarejo, M.F.; Barrera, J.; García, G.; Borja, R. Kinetics of phosphorus removal and struvite formation by the utilization of by-product of magnesium oxide production. *Chem. Eng. J.* **2005**, *111*, 45–52. [CrossRef]
36. Rahaman, M.S.; Ellis, N.; Mavinic, D.S. Effects of various process parameters on struvite precipitation kinetics and subsequent determination of rate constants. *Water Sci. Technol.* **2008**, *57*, 647–654. [CrossRef]
37. Nelson, N.O.; Mikkelsen, R.L.; Hesterberg, D.L. Struvite precipitation in anaerobic swine lagoon liquid: Effect of pH and Mg:P ratio and determination of rate constant. *Bioresour. Technol.* **2003**, *89*, 229–236. [CrossRef]
38. Le Corre, K.S.; Valsami-Jones, E.; Hobbs, P.; Parsons, S.A. Kinetics of Struvite Precipitation: Effect of the Magnesium Dose on Induction Times and Precipitation Rates. *Environ. Technol.* **2007**, *28*, 1317–1324. [CrossRef]
39. Crutchik, D.; Garrido, J.M. Kinetics of the reversible reaction of struvite crystallisation. *Chemosphere* **2016**, *154*, 567–572. [CrossRef]
40. Wang, H.; Tian, Z.; Wang, H.; Yan, Q. Optimization and reaction kinetics analysis for phosphorus removal in struvite precipitation process. *Water Environ. Res.* **2020**, *92*, 1162–1172. [CrossRef]
41. Ge, K.; Ji, Y.; Tang, S. Crystallization Kinetics and Mechanism of Magnesium Ammonium Phosphate Hexahydrate: Experimental Investigation and Chemical Potential Gradient Model Analysis and Prediction. *Ind. Eng. Chem. Res.* **2020**, *59*, 13799–13809. [CrossRef]
42. Bhuiyan, M.; Mavinic, D.S.; Beckie, R.D. Dissolution kinetics of struvite pellets grown in a pilot-scale crystallizer. *Can. J. Civ. Eng.* **2009**, *36*, 550–568. [CrossRef]
43. Harrison, M.L.; Johns, M.R.; White, E.T.; Mehta, C.M. Growth Rate Kinetics for Struvite Crystallisation. *Chem. Eng. Trans.* **2011**, *25*, 309–314.
44. Li, X.Z.; Zhao, Q.L.; Hao, X.D. Ammonium removal from landfill leachate by chemical precipitation. *Int. J. Innov. Res. Dev.* **2014**, *19*, 409–415. [CrossRef]
45. Ariyanto, E.; Ang, H.M.; Sen, T.K. Effect of initial solution pH on solubility morphology of and struvite crystal. In Proceedings of the CHEMECA Conference, Sydney, NSW, Australia, 18–21 September 2011.
46. Doyle, J.D.; Parsons, S.A. Struvite formation, control and recovery. *Water Res.* **2002**, *36*, 3925–3940. [CrossRef]
47. Ariyanto, E.; Sen, T.K.; Ang, H.M. The influence of various physico-chemical process parameters on kinetics and growth mechanism of struvite crystallisation. *Adv. Powder Technol.* **2014**, *25*, 682–694. [CrossRef]
48. Prywer, J.; Sadowski, R.R.; Torzewska, A. Aggregation of Struvite, Carbonate Apatite, and Proteus mirabilis as a Key Factor of Infectious Urinary Stone Formation. *Cryst. Growth Des.* **2015**, *15*, 1446–1451. [CrossRef]
49. Matynia, A.; Koralewska, J.; Wierzbowska, B.; Piotrowski, K. The influence of process parameters on struvite continuous crystallization kinetics. *Chem. Eng. Commun.* **2006**, *193*, 160–176. [CrossRef]
50. Kozik, A.; Hutnik, N.; Piotrowski, K.; Mazienczuk, A.; Matynia, A. Precipitation and Crystallization of Struvite from Synthetic Wastewater under Stoichiometric Conditions. *Adv. Chem. Eng. Sci.* **2013**, *3*, 20–26. [CrossRef]
51. Hendrix, M.; Grasel, P.; Martin, L.; Tawfiq, K.; Chen, G. Ammonia removal from landfill leachate by struvite precipitation/coated silica sand filtration. *Environ. Waste Manag.* **2015**, *15*, 201. [CrossRef]
52. Kumar, R.; Pal, P.; Pal, P. Turning hazardous waste into value-added products: Production and characterization of struvite from ammoniacal waste with new approaches. *J. Clean. Prod.* **2013**, *43*, 59–70. [CrossRef]
53. Gong, W.; Li, Y.; Luo, L.; Luo, X.; Cheng, X.; Liang, H. Application of Struvite-MAP Crystallization Reactor for Treating Cattle Manure Anaerobic Digested Slurry: Nitrogen and Phosphorus Recovery and Crystal Fertilizer Efficiency in Plant Trials. *Int. J. Environ. Res. Public Health* **2018**, *15*, 1397. [CrossRef] [PubMed]
54. Siciliano, A.; Siciliano, A.; Siciliano, A. Assessment of fertilizer potential of the struvite produced from the treatment of methanogenic landfill leachate using low-cost reagents. *Env. Sci. Pollut. Res. Int.* **2016**, *23*, 5949–5959. [CrossRef] [PubMed]
55. AHutnik, N.; Kozik, A.; Mazienczuk, A.; Piotrowski, K.; Wierzbowska, B.; Matynia, A. Phosphates (V) recovery from phosphorus mineral fertilizers industry wastewater by continuous struvite reaction crystallization process. *Water Res.* **2013**, *47*, 3635–3643. [CrossRef]
56. Giesen, A.; Giesen, A.; Giesen, A. Crystallisation Process Enables Environmental Friendly Phosphate Removal at Low Costs. *Environ. Technol.* **2010**, *20*, 769–775. [CrossRef]

57. Capdevielle, A.; Sýkorová, E.; Biscans, B.; Béline, F.; Daumer, M.-L. Optimization of struvite precipitation in synthetic biologically treated swine wastewater—Determination of the optimal process parameters. *J. Hazard. Mater.* **2013**, *244–245*, 357–369. [CrossRef]
58. Doyoung, K.; Ch Ara, O.; Mccoy, C.P.; Irwin, N.J.; Rimer, J.D. Time-Resolved Dynamics of Struvite Crystallization: Insights from the Macroscopic to Molecular Scale. *Chemistry* **2020**, *26*, 3555–3563. [CrossRef]
59. Galbraith, S.C.; Schneider, P.A.; Flood, A.E. Model-driven experimental evaluation of struvite nucleation, growth and aggregation kinetics. *Water Res.* **2014**, *56C*, 122–132. [CrossRef]
60. Koralewska, J.; Piotrowski, K.; Wierzbowska, B.; Matynia, A. Reaction—Crystallization of Struvite in a Continuous Liquid Jet—Pump DTM MSMPR Crystallizer with Upward Circulation of Suspension in a Mixing Chamber—An SDG Kinetic Approach. *Chem. Eng. Technol.* **2010**, *30*, 1576–1583. [CrossRef]
61. Hakimi, M.H.; Jegatheesan, V.; Navaratna, D. The potential of adopting struvite precipitation as a strategy for the removal of nutrients from pre-AnMBR treated abattoir wastewater. *J. Environ. Manag.* **2020**, *259*, 109783. [CrossRef]
62. Le Corre, K.S.; Valsami-Jones, E.; Hobbs, P.; Parsons, S.A. Phosphorus Recovery from Wastewater by Struvite Crystallization: A Review. *Crit. Rev. Environ. Sci. Technol.* **2009**, *39*, 433–477. [CrossRef]
63. Yaakoubi, M.; Kinoshita, S.; Liu, B.; Ha, N.T.; Van, L. Modelling Multiple Mineral Precipitation in Anaerobic Digestion Process. In Proceedings of the 7th IWA-ASPIRE Conference and Exhibition, Kuala Lumpur, Malaysia, 13–16 September 2017.
64. Hutnik, N.; Stanclik, A.; Piotrowski, K.; Matynia, A. Effect of Copper and Zinc Ions on Struvite Nucleation and Crystal Growth Kinetics in Various Process Environments. *Pol. J. Environ. Stud.* **2020**, *29*, 2225–2233. [CrossRef]
65. Hutnik, N.; Stanclik, A.; Piotrowski, K.; Matynia, A. Size-dependent growth kinetics in continuous struvite reaction crystallization in wastewaters and cattle liquid manure with potassium ions. *Przem. Chem.* **2019**, *98*, 644–649. [CrossRef]
66. Ping, Q.; Li, Y.; Wu, X.; Yang, L.; Wang, L. Characterization of morphology and component of struvite pellets crystallized from sludge dewatering liquor: Effects of total suspended solid and phosphate concentrations. *J. Hazard. Mater.* **2016**, *310*, 261–269. [CrossRef]
67. Li, S.; Zeng, W.; Xu, H.; Jia, Z.; Peng, Y. Performance investigation of struvite high-efficiency precipitation from wastewater using silicon-doped magnesium oxide. *Environ. Sci. Pollut. Res.* **2020**, *27*, 15463–15474. [CrossRef] [PubMed]
68. Song, Y.; Dai, Y.; Hu, Q.; Yu, X.; Qian, F. Effects of three kinds of organic acids on phosphorus recovery by magnesium ammonium phosphate (MAP) crystallization from synthetic swine wastewater. *Chemosphere* **2014**, *101*, 41–48. [CrossRef]
69. Zhang, Q.; Zhao, S.; Ye, X.; Xiao, W. Effects of organic substances on struvite crystallization and recovery. *Desalination Water Treat.* **2015**, *57*, 10924–10933. [CrossRef]
70. Zhou, Z.; Hu, D.; Ren, W.; Zhao, Y.; Jiang, L.M.; Wang, L. Effect of humic substances on phosphorus removal by struvite precipitation. *Chemosphere* **2015**, *141*, 94–99. [CrossRef]